AIAA JOURNAL
Vol. 42, No. 5, May 2004

Fluid Dynamics of Highly Pitched and Yawed Jets in Crossflow

Ivana M. Milanovic*
University of Hartford, West Hartford, Connecticut 06117
and
K. B. M. Q. Zaman†
NASA John H. Glenn Research Center at Lewis Field, Cleveland, Ohio 44135

Results from an experimental investigation of flowfields generated by pitched and yawed jets discharging into a crossflow are presented. The circular jet is pitched at $\alpha = 20$ and 45 deg and yawed between $\beta = 0$ and 90 deg in increments of 15 deg. Hot-wire measurements are performed to obtain all three components of mean velocity and turbulent stresses. Cross-sectional surveys are conducted at $x = 3$, 5, 10, and 20, where the downstream distance x is normalized by the orifice diameter. Data are acquired at momentum-flux ratio, $J = 1.5$, 4, 8, and 20. As expected, the jet penetration is found to be higher at larger α. With increasing β the jet spreads more. The rate of decrease of peak streamwise vorticity, $\partial\omega_{x\,\max}/\partial x$, is found to be significantly lower at higher β but practically independent of α. Thus, at the farthest measurement station, $x = 20$, $\omega_{x\,\max}$ is about five times larger at $\beta = 75$ deg compared to that at $\beta = 0$ deg. Streamwise velocity within the jet-vortex structure is found to depend on the parameter J. At $J = 1.5$ and 4, wake-like velocity profiles are observed. In comparison, a jet-like overshoot is present at higher J. Distributions of turbulent stresses for various cases are documented. Regions of high normal stresses, dispersed initially, are eventually ingested by the streamwise vortices. Thus, at $x = 10$ and farther downstream the well-defined cores of the streamwise vortices are also the zones of highest turbulent activity.

Nomenclature

D	=	nozzle diameter
J	=	momentum-flux ratio, $J = (\rho_j U_j^2)/(\rho_\infty U_\infty^2)$
U	=	mean jet or freestream velocity normalized by U_∞
u, v, w	=	mean velocity in streamwise, normal and spanwise directions normalized by U_∞
u', v', w'	=	turbulence intensities normalized by U_∞
$\overline{u'v'}$	=	turbulent shear stress normalized by U_∞^2
VR	=	velocity ratio, $VR = U_j/U_\infty$
x, y, z	=	Cartesian coordinates normalized by D
α	=	jet pitch angle relative to tunnel floor, degrees
β	=	jet yaw angle relative to direction of cross-flow, degrees
ρ	=	density
ω	=	vorticity normalized by U_∞/D

Subscripts

j	=	jet
max	=	maximum
∞	=	freestream

Introduction

JETS in crossflow (JICF) have applications in a variety of technologically important systems and processes. In one form or another JICF is involved in active flow control, aircraft performance and stability, mixing augmentation, film and effusion cooling, etc. Before discussing the objectives of this study, we will review the flow features of JICF and some pertinent work from the literature. The presence of the high-momentum transverse jet in a crossflow has a similar effect as that of a solid body. The retarded flow at the jet's leading edge creates an increased pressure, while the trailing edge is characterized by low pressure. The crossflow deflects the jet into its characteristic trajectory and deforms the jet cross section. At the same time, the crossflow shears the jet fluid around its perimeters, and the resulting vorticity redistribution ultimately develops into a counter-rotating vortex pair. It has been shown that this streamwise vortex pair, which is a salient feature of a JICF, can persist for hundreds of jet diameters downstream.

Investigation of the flowfield of an inclined JICF dates back to 1952, when Wallis[1] showed that a pitched and yawed jet produces a vortex system similar to one from a wing-type vortex generator. Wu et al.[2] used flow visualization to document the flow topology of normal jets with different cross-sectional shape for $1 \le VR \le 9$. Note that for incompressible single gas flow the velocity ratio VR is the square root of the momentum-flux ratio J. In Ref. 2, comparisons of flowfields were made in an attempt to identify conditions that enhance asymmetry. Johnston and Nishi[3] studied jets pitched at 45 deg and yawed at 90 and 180 deg over the range of velocity ratios, $0.4 \le VR \le 1$. (Figure 1 defines yaw and pitch angles.) The emphasis was on the exploration of an alternative to solid vortex generators for flow control. Lin et al.[4] examined 45-deg pitched jets for $1.7 \le VR \le 6.8$, as part of a comparative study on passive and active methods for flow control. Compton and Johnston[5] investigated mean velocity field at $\alpha = 45$ deg and for β up to 180 deg, over the VR range of 0.7–1.3. The study indicated that an optimal yaw angle producing maximum vorticity might be between 45 and 90 deg. Selby et al.[6] conducted a parametric study of a streamwise array of JICF placed upstream of a rearward-facing ramp. Pitch angle was varied between 15 and 90 deg, and the yaw between 0 and 90 deg, over the VR range of 0.6–6.8. The results showed that the effectiveness of separation control depended on jet velocity, location, and orientation. Honami et al.[7] carried out an investigation of a jet at $\alpha = 30$ deg, $\beta = 90$ deg, and $0.5 \le VR \le 1.2$, for film-cooling purposes. An increase in velocity ratio was shown to enhance asymmetry of the vortical system and reduce film-cooling effectiveness.

While the aforementioned research focused on the mean flow features, Zhang[8] obtained data on turbulent stresses for pitch and yaw

Presented as Paper 2003-0183 at the 41st Aerospace Sciences Meeting, Reno, NV, 6–9 January 2003; received 6 June 2003; revision received 17 November 2003; accepted for publication 19 November 2003.

*Assistant Professor, College of Engineering, Technology and Architecture, 200 Bloomfield Avenue; Milanovic@hartford.edu. Member AIAA.

†Aerospace Engineer, Turbomachinery and Propulsion Systems Division, Nozzle Branch, 21000 Brookpark Road, M.S. 86-7; Khairul.B.Zaman@nasa.gov. Associate Fellow AIAA.

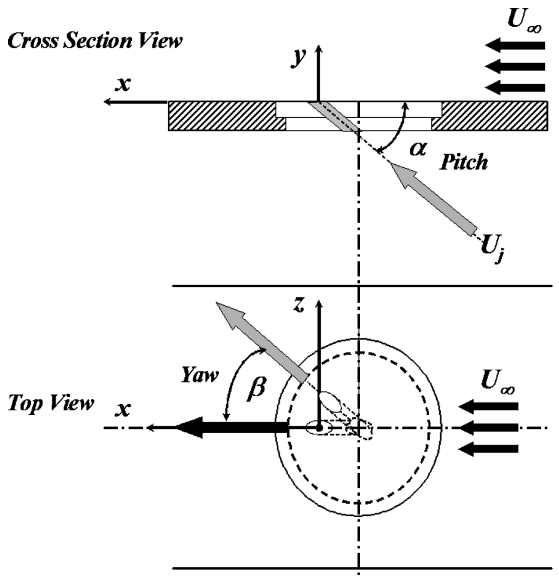

Fig. 1 Experimental setup.

angles of 45 deg at velocity ratios up to 1.5, using laser Doppler anemometry (LDA). Johnston and coworkers[9–11] performed flow visualization as well as LDA measurements at $\alpha = 30$ and 45 deg, $\beta = 45$–90 deg, and $1 \leq VR \leq 1.5$. Quantitative information on the flowfield included both mean and turbulent flow features. It was found that for a velocity ratio of 1, 30-deg pitch, and 60-deg yaw produced the vortex with the maximum mean vorticity. Jonhston[12] reviewed experimental and computational results on pitched and yawed JICF. For effect on boundary-layer detachment, the velocity ratio of the JICF was inferred to be a key parameter; $VR = 1$ affected almost complete reattachment, and lower values reduced the size of the stall bubble. Bray[13] performed detailed five-hole probe surveys examining effects of pitch angle, yaw angle, diameter as well as Mach-number ratio, for the range $0.7 < VR < 2$. Comparisons between vane and airjet vortices were also made. Bray and Garry[14] presented a correlation for maximum vorticity of a pitched and yawed JICF.

It is obvious that a lot of work has been done in the subject area. Yet, because of the vast parameter space a coherent understanding has been lacking. Many aspects of the flowfield such as the structure, trajectory, and evolution of the streamwise vortices as a function of pitch and yaw angles and momentum-flux ratio, remain far from being completely clear. Moreover, the literature lacks detailed measurements at low pitch, high-momentum flux ratio and with enhanced angular resolution in yaw. Such information is increasingly in demand by the designer of propulsion components. This provided the motivation for revisiting the subject and carrying out the present study. The objective was to obtain detailed quantitative data on the flowfield evolution for systematic variation of parameters, as elaborated in the following.

The current manuscript is a revised and refined version of an earlier conference paper.[15] Only key results are presented here to highlight the main inferences. The discussion in the following, however, will draw on the entire dataset and comparison will be made with data from the literature wherever possible.

Experimental Setup

The investigation was conducted in a NASA Glenn Research Center open-circuit, low-speed wind tunnel with a 0.76 m wide × 0.51 m high test section. The tunnel had the fan on the downstream end and a 16:1 contraction section together with five flow conditioning screens yielded less than 0.1% turbulence intensity in the freestream. The jet was produced with an inclined nozzle of diameter $D = 19$ mm. The nozzle was a straight orifice cut through a clear plastic disk of 25.4 mm thickness. The disk was mounted flush on the test-section floor. The setup is shown schematically in Fig. 1. Compressed air supplied through a flexible hose passed through a 20-cm-long pipe section and a wire-mesh screen before entering the nozzle. The resultant flow at the exit of the nozzle was uniform in the absence of the crossflow; however, the turbulence intensity was high, about 16% throughout the core. An orifice meter fitted to the supply line was used to monitor the mass flow rate that was used to calculate the mean jet velocity U_j.

The disk with the orifice was placed centrally near the beginning of the test section, and the measurement domain was within one test-section height. Thus, tunnel wall effects on the data are considered insignificant. Two disks were used to provide two pitch angles, ($\alpha = 20$ and 45 deg), measured between the orifice axis and the floor of the test section. Each disk could be rotated to vary the yaw angle β, measured between the orifice axis and the direction of the crossflow. The jet was yawed in 15-deg increments between 0 and 90 deg.

The measurements on a cross-sectional plane of the jet at various streamwise locations were performed using two adjacent ×-film probes (TSI 1241-20), one placed in u–v and the other in u–w orientation. The probes were traversed under automated computer control through the same grid points. The probe traverse had a minimum step of 0.025 mm; however, the sensor length of about 1 mm dictated the spatial resolution of the measurements. Appropriate relative shift of the two datasets from the two probes yielded the distribution of all three components of velocity and turbulence intensities on a given cross-sectional plane. The v and w data were corrected for the error introduced by the u gradients and finite separation of the sensors in each probe. The probes were calibrated in situ, and the outputs from the four sensors were least-squares fitted with fourth-order polynomials as a function of the tunnel velocity. The polynomial coefficients were later used to calculate the velocities using cosine law. Except for the upstream-most location and at highest jet velocities, the flow angularity was within 20 deg. Pitch and yaw corrections were not invoked. The errors introduced in v and w as a result of 20-deg flow angularity were within 5%, as indicated by an earlier study in the same facility.[16] During data acquisition the freestream velocity was monitored constantly. If there was more than 1% deviation, the acquisition was stopped. Data normalization was done by updated value of U_∞. However, because of the long durations of the surveys some drift in the hot-wire calibration was inevitable. This turned out to be the most significant contributor to the uncertainty in the data. The uncertainty in the normalized u velocity is estimated to be within 2%. Uncertainty in the mean streamwise vorticity ω_x, obtained from the gradients of the corrected v and w, is estimated to be about 20%. Some further details of the facility and hot-wire procedure can be found in Ref. 16.

The origin of the coordinate system is located at the center of the jet orifice. The streamwise (i.e., the crossflow) direction is denoted by x, the direction normal to the tunnel floor is denoted by y, and the spanwise direction along the tunnel floor by z (Fig. 1). A saw-tooth boundary-layer trip was applied at the beginning of the test section. Cursory surveys at a fixed location indicated that the approach boundary layer transitioned around $U_\infty = 4$ m/s. All data were acquired for a constant freestream velocity of $U_\infty = 8$ m/s so that the approach boundary layer was fully turbulent. The profiles measured at $x = -0.5$ and $z = 2$ are shown in Fig. 2. The boundary-layer thickness at this location is about 0.4 jet diameters. The Reynolds number, based on U_∞ and orifice diameter, is 9.8×10^3. Most of the data were acquired at $J = 8$ chosen such that the jet trajectory was in the middle of the measurement domain and not too close to either the floor or the ceiling of the test section. Data for all pitch and yaw configurations were acquired at $x = 3$, 5, 10, and 20. Additionally, for $J = 1.4$, 4, and 20 surveys were conducted at $x = 10$ for $\alpha = 10$ and 45 deg and $\beta = 75$ deg. The test matrix involved a total of 48 cross-sectional surveys.

Results and Discussion

Mean Velocities

Contours of streamwise velocity distribution u for 20-deg pitch and zero yaw at $J = 8$ are presented in Fig. 3. A symmetrical distribution around the $z = 0$ plane is noted. Crossflow vectors (v, w), shown as constant length arrows, indicate strong lateral flow toward

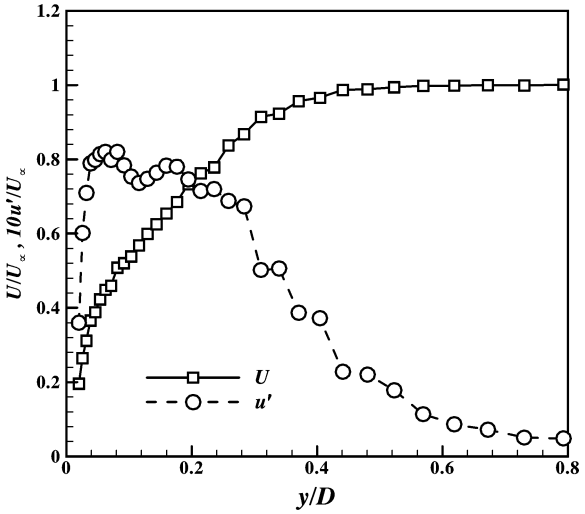

Fig. 2 Approach boundary-layer characteristics; $x = -0.5$ and $z = 2$.

the symmetry plane. As the fluid passage is restricted by the wall and the symmetry condition, flow is forced upward deforming the jet into a kidney shape. Corresponding data for $\alpha = 45$ deg have been presented in Ref. 15. For a given downstream location, the upward penetration of the jet and the curvature of the jet cross section are more pronounced at the higher pitch angle. Salient differences for the two cases will be discussed further with the help of profiles of various flowfield properties.

Streamwise velocity contours for a representative yawed case ($\alpha = 20$, $\beta = 75$ deg, and $J = 8$) are shown in Fig. 4, capturing the evolution of the jet cross section with increasing downstream distance. A comparison with Fig. 3 reveals that the yawed jet has spread more, as indicated by the area under a given contour on the outer edge of the jet. A distorted kidney shape is first discernible. With increasing x, the structure has rotated counterclockwise, and the maximum velocity has shifted farther away from the tunnel centerline (initial jet location). The region of peak velocity on the right has lifted and diminished in magnitude, and far downstream only one local maximum has remained. Also, peak velocities are closer to the wall and have considerably lower values compared to the zero yaw case. Overall, the flowfield for $\alpha = 45$ deg and $\beta = 75$ deg has a similar behavior of outward translation and simultaneous counterclockwise rotation with downstream distance.

In Fig. 5, the influence of momentum-flux ratio, for a given pitch and yaw, is examined at a fixed downstream location ($x = 10$). It can be seen that the jet-vortex field at values of J greater than about 4 are characterized by velocities higher than U_∞. On the other hand, velocity deficits are observed at lower values of J. A deficit was also seen for $J = 1$ in the works of Compton and Johnston,[5] Khan and Johnston,[10] Johnston et al.,[11] and Lee et al.[17] Gopalan et al.[18] reported a fundamental change in the flow structure across a threshold of J of about 2. The present results not only confirm the velocity deficit at low J, but also capture a systematic trend. Velocity overshoot becomes the prominent feature at higher J. Note that at intermediate values of J both deficit and overshoot take place within the jet-vortex structure. The present results, obtained up to $x = 20$, moreover, indicate that the velocity deficit at low J can persist farther downstream than previously noted.

To characterize the overall evolution of the flowfields, peak streamwise velocity obtained from each cross-sectional field ($u_{\max}$) is examined. Variations of $u_{\max}$ with x for four representative cases are shown in Fig. 6. It can be seen by comparing data at a given α that a higher yaw results in lower velocities at all measurement stations. On the other hand, for a given β velocities are lower at higher pitch. Figure 7 shows variations of $u_{\max}$ with the yaw angle for two values of α and for two measurement stations x. A systematic trend can be observed. The peak velocity decreases with increasing yaw. At the downstream location ($x = 10$) the variation is almost linear. Although simplistic, data as in Figs. 6 and 7 could be useful to a designer. The detailed flowfields, however, are complex. For example, the location of $u_{\max}$ is found to shift upward with higher pitch and outwards with higher yaw.

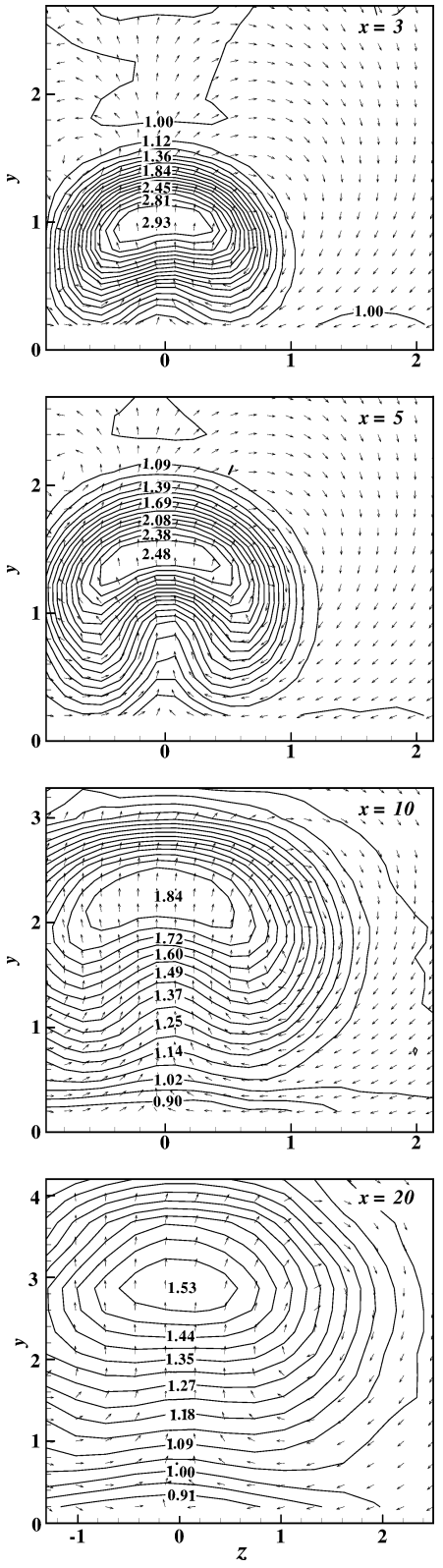

Fig. 3 Downstream evolution of streamwise velocity distribution; $\alpha = 20$ deg, $\beta = 0$ deg, and $J = 8$.

Recall that at low J, the jet-vortex structure is characterized by velocity deficit (Fig. 5). This is examined further in Fig. 8. Velocity profiles through the point of minimum u are shown in this figure for $J = 1.5$ at $x = 10$. At zero yaw, velocity profiles for both pitch values exhibit one local minimum and one local maximum. The magnitude

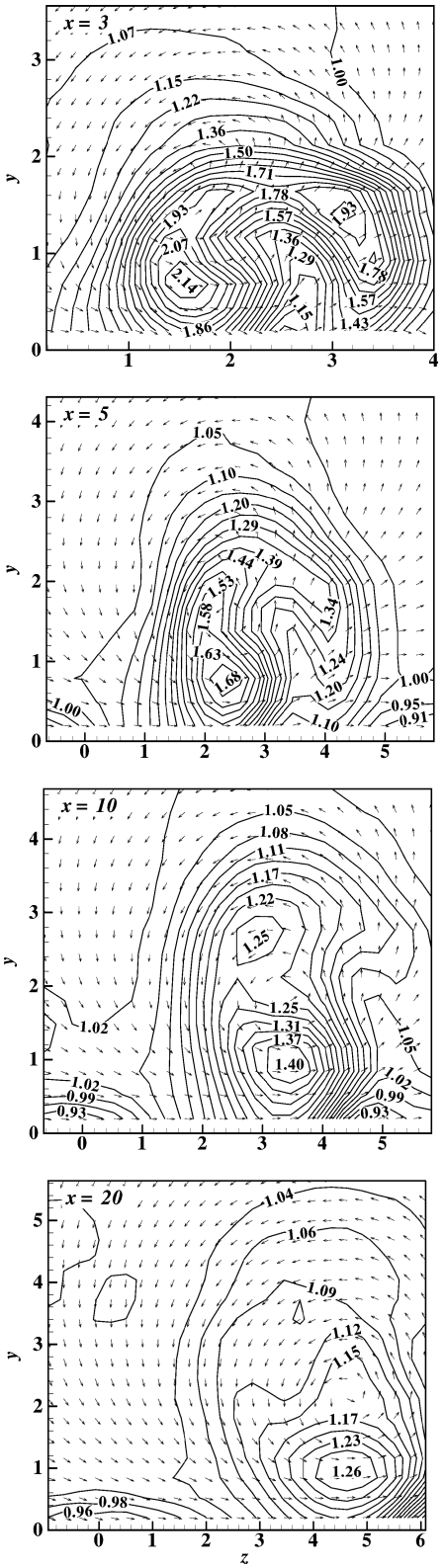

Fig. 4 Downstream evolution of streamwise velocity distribution; $\alpha = 20$ deg, $\beta = 75$ deg, and $J = 8$.

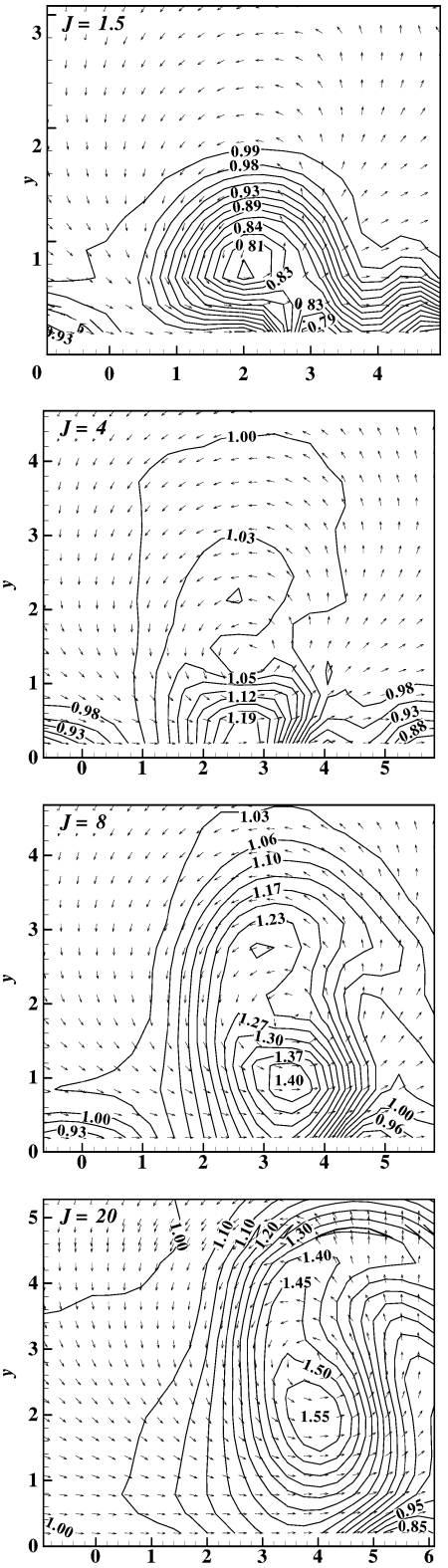

Fig. 5 Streamwise velocity distribution for various momentum-flux ratios; $\alpha = 20$ deg, $\beta = 75$ deg, and $x = 10$.

of the minima for both pitch are comparable, $u \approx 0.85$, the one at higher pitch occurring farther away from the wall. The profiles for the 75-deg yaw case have one pronounced minimum, 0.69 for 20-deg pitch, and 0.79 for 45-deg pitch. These minima coincide with the core of the stronger vortex. At this high yaw angle, the weaker vortex has already been diffused. The deficit values compare well with the measurements of Khan and Johnston[10] and Johnston et al.[11] A configuration with $\alpha = 30$ deg and $\beta = 60$ deg in Ref. 11, exhibited velocity minima of 0.7 and 0.85, at $x = 10$, for $J = 1$ and 2.25, respectively.

Mean Streamwise Vorticity

Contours of streamwise vorticity distribution ω_x for the configurations of Fig. 4 are presented in Fig. 9. For this case of large yaw, the vortex with the positive vorticity becomes the dominant structure with increasing downstream distance. Its strength at $x = 5$, for

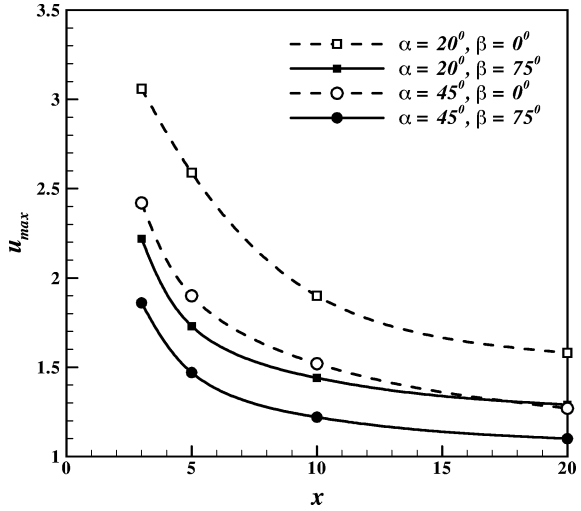

Fig. 6 Maximum streamwise velocities at various measurement planes; $J = 8$.

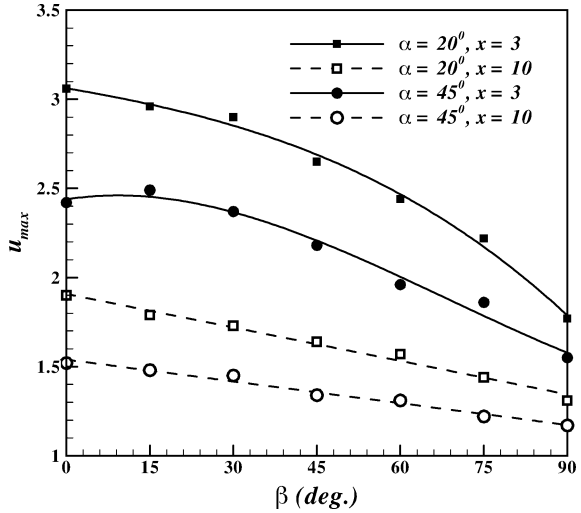

Fig. 7 Maximum streamwise velocities vs yaw angle; $J = 8$.

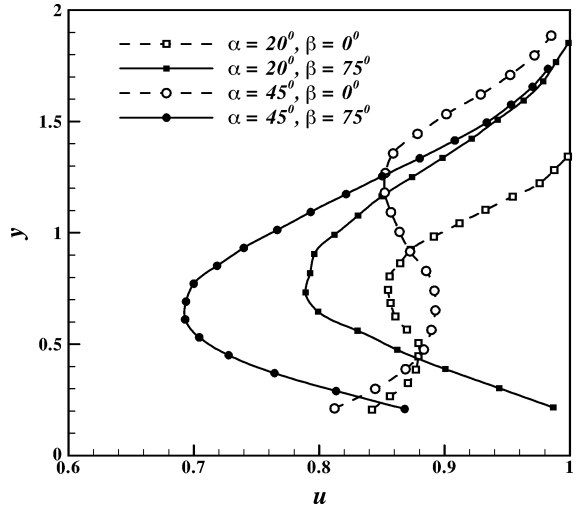

Fig. 8 Velocity profiles through the point of minimum velocity; $J = 1.5$ and $x = 10$.

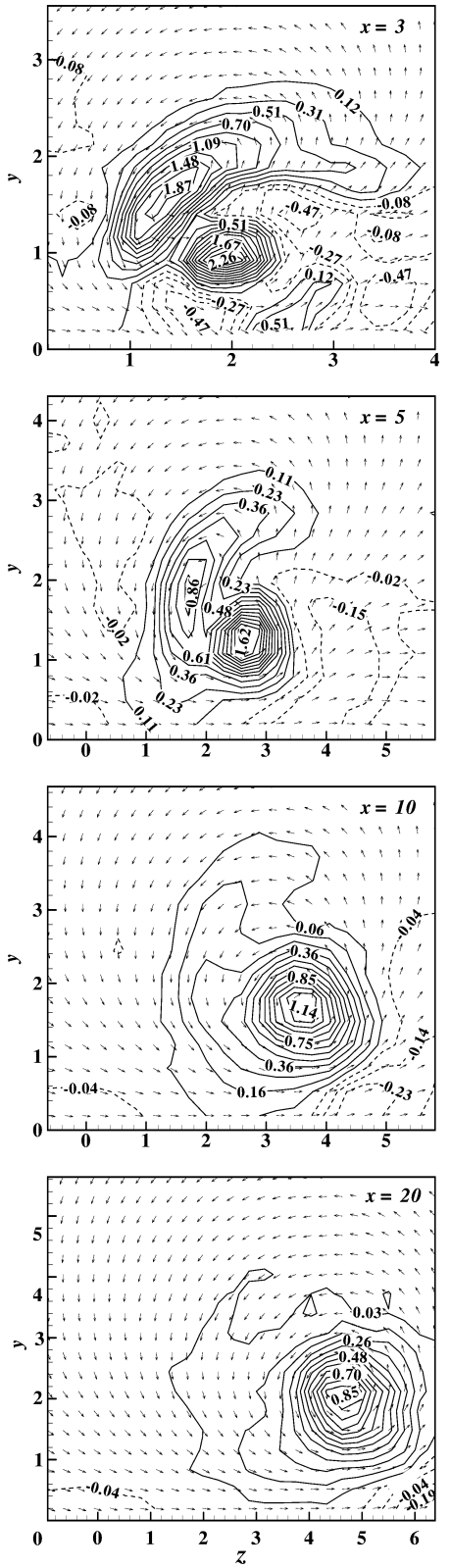

Fig. 9 Downstream evolution of streamwise vorticity distribution; $\alpha = 20$ deg, $\beta = 75$ deg, and $J = 8$.

example, is six times that of the negative vortex. There is also a net transport of the vortex system laterally in the yawed direction. At the upstream locations additional concentrations of negative vorticity are observed near the wall, presumably because of reorientation of the boundary layer. The regions of concentrated negative vorticity are then quickly diffused farther downstream. At the last measurement station, essentially a single vortex with positive vorticity remains. In the case of zero yaw, the counter-rotating vortex

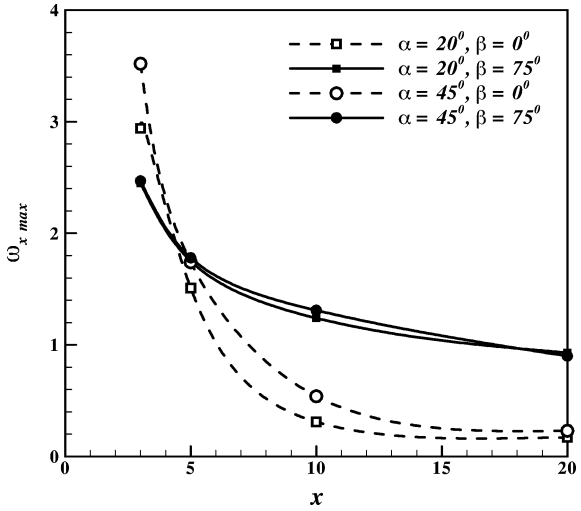

Fig. 10 Maximum streamwise vorticity as a function of downstream distance; $J = 8$.

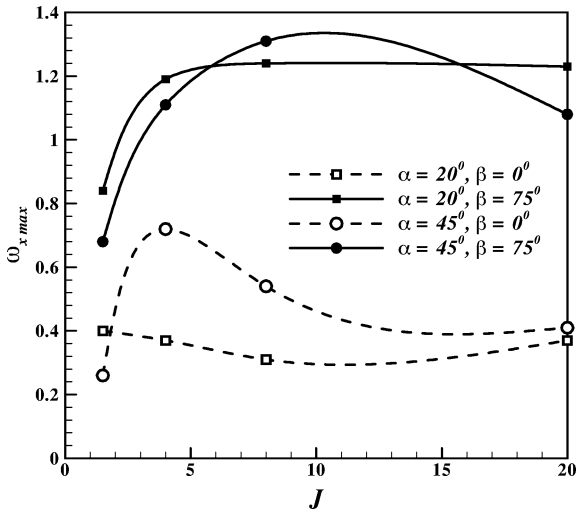

Fig. 11 Maximum streamwise vorticity as a function of momentum-flux ratio; $x = 10$.

pair moves away from the wall and apart from each other with increasing x, but both vortices are still detectable at $x = 20$. However, the magnitude of each component is much smaller than that of the vortex for the yawed case, and this can be observed in the profiles shown next.

As with the velocity data, peak streamwise vorticity $\omega_{x\,\max}$ from each cross-sectional field is now examined. An inspection of Fig. 9 reveals that $\omega_{x\,\max}$ decreases with downstream distance. This is clearly seen in Fig. 10 for both pitch cases. At zero yaw $\omega_{x\,\max}$ is found to become half of the initial value by $x = 5$, and by the last measurement station it is reduced to about one-tenth. The rate of decrease for $\beta = 75$ deg is more gradual and a vortex of considerable strength remains at $x = 20$. It is also clear that the magnitudes at different pitch but same yaw compare closely. These results also appear to be characteristic of a range of J investigated in the present experiments, as clearly evident from the data shown in Fig. 11. For a given yaw, the changes in $\omega_{x\,\max}$ are small when the momentum-flux ratio is increased beyond a value of about four. On the other hand, higher yaw results in higher $\omega_{x\,\max}$ at all J. Thus, if an application requires longer persistence of streamwise vorticity yawed jets are clearly advantageous. Note that the curves are merely smooth fits through the limited data, and not much further could be inferred about the trends.

Referring back to Fig. 9, it is noted that at the first measurement station there are two regions of loosely dispersed positive

Table 1 Maximum turbulence intensities at various downstream locations, where $\alpha = 20$ deg and $J = 8$

x	$u'_{\max}$	$v'_{\max}$	$w'_{\max}$
	$\beta = 0$ deg		
3	0.474	0.441	0.353
5	0.460	0.423	0.324
10	0.318	0.299	0.257
20	0.192	0.199	0.196
	$\beta = 75$ deg		
3	0.563	0.472	0.399
5	0.385	0.313	0.338
10	0.231	0.208	0.223
20	0.161	0.168	0.173

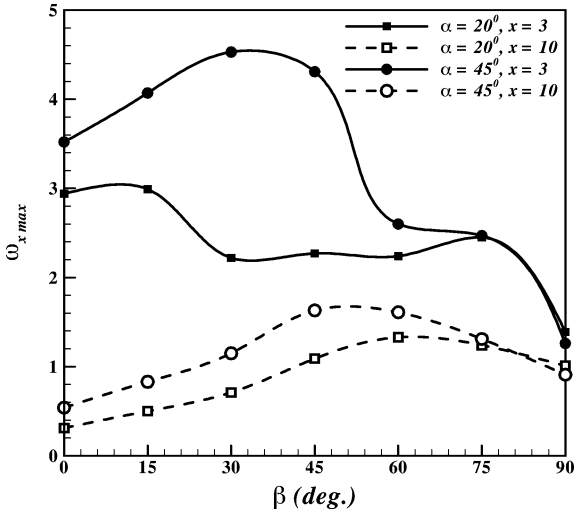

Fig. 12 Maximum streamwise vorticity as a function of yaw angle; $J = 8$.

vorticity. Although we conjectured before that the origin of the additional regions of negative vorticity is caused by boundary-layer reorientation, the origin of the additional positive vortex remains unclear. However, such an occurrence was also noted in Ref. 10 at $J = 1$, $\alpha = 30$ deg, and $\beta = 60$ deg. Obviously, the flow is in an early stage of the rolling-up process. It is plausible that the two regions are caused by reorientation of different segments of the elliptic shear layer that is issued into the crossflow. With increasing downstream distance these two regions merge, and by $x = 10$ only one well-defined vortex is left.

The variation of peak streamwise vorticity as a function of yaw angle for the positive vortex is summarized in Fig. 12 for $J = 8$, at $x = 3$ and 10. At the upstream location the trends are complex because the field is still evolving. At $x = 10$, however, a clear picture has emerged. There is a marked dependence of $\omega_{x\,\max}$ on β. The maxima for $\alpha = 20$ and 45 deg are found at $\beta = 60$ and 45 deg, respectively. A similar observation was made in Ref. 11 for $J = 1$. This result should be useful providing a guideline for the choice of yaw angles when desiring the strongest streamwise vortices in applications.

Turbulent Stresses

Contour plots of turbulent stresses (nondimensionalized by U_∞) are presented for the same combinations of parameters as considered in the preceding sections. The distributions of streamwise turbulence intensity, corresponding to the case of Figs. 4 and 9, are shown in Fig. 13. Peak field values for all three turbulence intensity components are summarized in Table 1. One finds that the peak magnitudes decrease with increasing distance. The peak value of u' is larger than those of v' and w' at the upstream locations. However, at $x = 20$ the levels have become comparable. Corresponding data for zero yaw (contours not shown) indicate that the turbulent structure changes its shape and spreads with increasing x, commensurate with the U

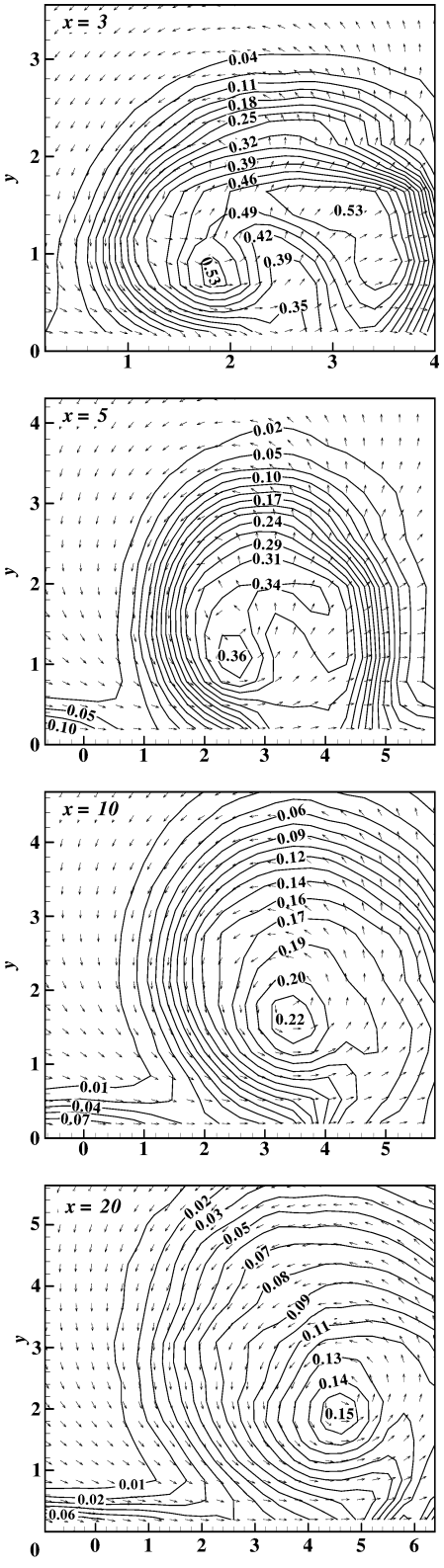

Fig. 13 Downstream evolution of streamwise turbulence intensity distribution; $\alpha = 20$ deg, $\beta = 75$ deg, and $J = 8$.

distributions. Also, a smaller pitch angle produces larger peaks in u'. The levels of peak turbulence intensities are in agreement with previous findings of Zhang[8] and Khan and Johnston.[10]

Comparison of Fig. 13 with Fig. 9 makes it clear that the areas of peak turbulence correspond to zones of concentrated vorticity. At $x = 3$ the regions of high turbulence intensity are dispersed as are the zones of concentrated vorticity. As the vortex rolls up into a well-defined core, the turbulence congregates into the core. Far downstream the location of peak turbulence coincides exactly with the location of peak vorticity. As to why turbulence congregates into the core of a streamwise vortex has been addressed before and a few explanations offered:

1) The core of a streamwise vortex entrains surrounding turbulence.[19]

2) The core acts as a wave guide propagating disturbances that would have otherwise dissipated.[20]

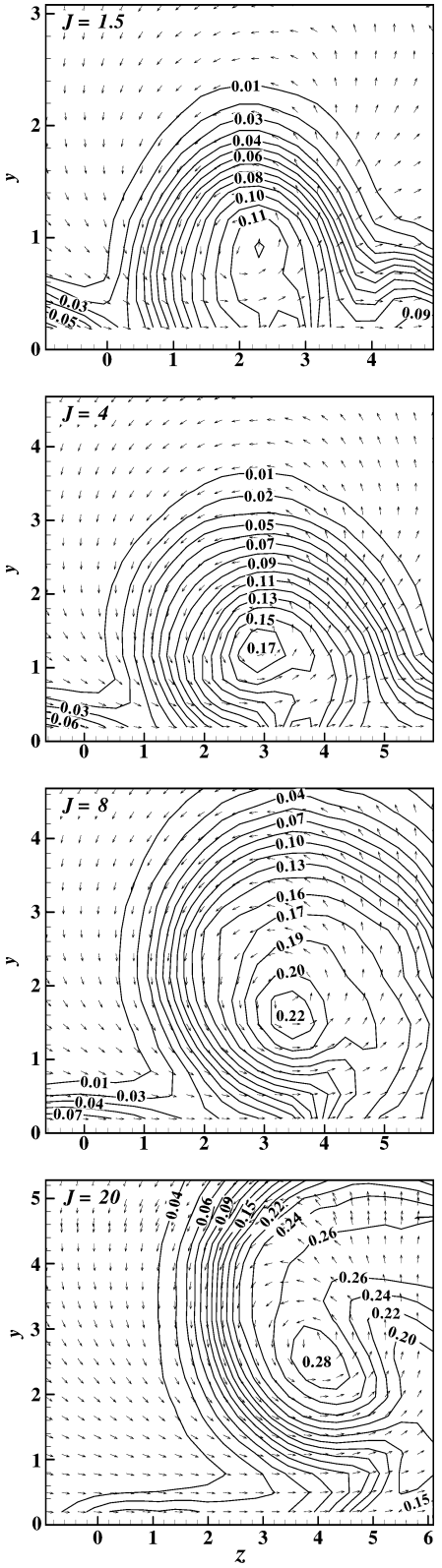

Fig. 14 Streamwise turbulence intensity distribution for various momentum-flux ratios; $\alpha = 20$ deg, $\beta = 75$ deg, and $x = 10$.

3) Vortex meandering could be the significant contributor to the high turbulence.[10]

The precise mechanism remains unclear; however, the trends of Fig. 13 support 1), that is, turbulence from the surrounding flow is ingested or entrained into the core as the vortex develops. The same observation was also made in an investigation of flowfields of a delta wing.[21]

Characteristic u' distributions for varying J are shown in Fig. 14. Data on maximum turbulence intensities for $\beta = 0$ and 75 deg are listed in Table 2. It is observed that peak values rise with increasing J. For $J = 1.5$ the vortex is in the proximity of the tunnel wall, and high turbulence encompasses the vortex core and the boundary layer beneath it. The proximity of the vortex to the wall energizes the boundary layer. That is expected to be beneficial for separation control. For J greater than 1.5, the region of maximum turbulence coincides with the core, although some high levels are still found beneath the vortex. As the vortex moves upward with increasing J, the boundary layer immediately below the core is affected less. Thus, for the given pitch and yaw there might be a threshold of J (approximately 4) below which the vortex-generating jets would be effective in energizing the boundary layer for separation control.

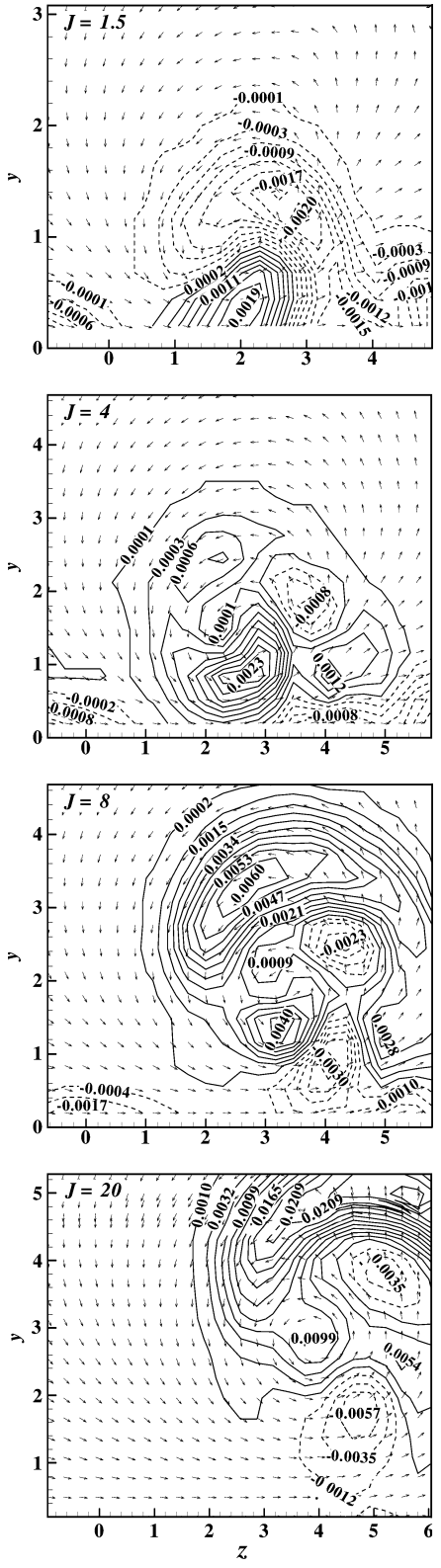

Fig. 15 Contours of $\overline{u'v'}$ for various momentum-flux ratios; $\alpha = 20$ deg, $\beta = 75$ deg, and $x = 10$.

Table 2 Maximum turbulence intensities at various momentum-flux ratios, where $\alpha = 20$ deg and $x = 10$

J	$u'_{\max}$	$v'_{\max}$	$w'_{\max}$
	$\beta = 0$ deg		
1.5	0.093	0.072	0.079
4	0.153	0.143	0.143
8	0.318	0.299	0.257
20	0.521	0.454	0.372
	$\beta = 75$ deg		
1.5	0.144	0.119	0.123
4	0.176	0.169	0.178
8	0.237	0.208	0.223
20	0.302	0.264	0.280

The measurements also included two shear-stress components. Only $\overline{u'v'}$ distribution, corresponding to the case of Figs. 5 and 14, is shown in Fig. 15. Unlike zero yaw where the positive and negative $\overline{u'v'}$ run alongside and almost parallel to the wall, the flowfield here has slanted the boundary between regions of positive and negative $\overline{u'v'}$. At low-momentum-flux ratio regions of positive and negative $\overline{u'v'}$ are located below and above the vortex core, respectively. This is the case when the core is characterized by the mean velocity deficit. The distributions as well as the levels agree with observations of Zhang[8] and Khan and Johnston.[10] Increasing J results in the mean velocity overshoot, negative $\overline{u'v'}$ in the boundary layer below the vortex, scattered patches of negative $\overline{u'v'}$ values around the vortex core, and finally positive $\overline{u'v'}$ region spread widely at the top. As with u' distributions, at low J there exists significant $\overline{u'v'}$ levels below the jet-vortex region near the wall. Thus, once again one infers that the yawed jet is effective in energizing the boundary layer below a threshold of about $J = 4$.

Summary

An experimental investigation of pitched and yawed jets in crossflow was carried out. To complement existing database in the literature, low pitch angle, high-momentum-flux ratios, and enhanced angular resolution in yaw were covered in this experiment.

The results reveal that yawed jets are advantageous for applications requiring longer persistence of streamwise vortices. For various $\alpha - J$ combinations, the strongest streamwise vortices are found to occur between 45- and 60-deg yaw. For the range of momentum-flux ratios examined, both velocity deficit and overshoot in the jet-vortex structure are observed. Although the mechanisms of deficit/overshoot remain unclear, a systematic dependence on J is observed. The deficit occurs for J less than about 4 while overshoot appears at higher J.

The distributions of turbulent stresses and change in their levels with pitch, yaw, and momentum-flux ratio are documented. In general there is anisotropy in the flow that is more pronounced at locations closer to the orifice. Peak normal stresses are found to occur within the vortex core. This is mainly a result of ingestion of turbulence from the surrounding flow. For same yaw, the smaller pitch angle produces larger peaks in u', v', and w'. Yawed jets are found to remain closer to the wall and enhance turbulence in the vicinity of the boundary layer. This effect is most pronounced in a lower range of momentum-flux ratios.

Acknowledgments

The work was supported by the NASA–Ohio Aerospace Institute Collaborative Aerospace Research and Fellowship Program. The first author is grateful to Connecticut Space Grant College Consortium-Experimental Program to Stimulate Competitive Research (EPSCoR) Core Funding for providing support. The authors are also thankful to Bruce Wendt of NASA Glenn Research Center and Frank Y. Wang of U.S. Department of Transportation/Volpe for the valuable discussions.

References

[1]Wallis, R. A., "The Use of Air Jets for Boundary Layer Control," Aerodynamics Research Labs., Aero Note 110, N-34736, Melbourne, Australia, Jan. 1952.

[2]Wu, J. M., Vakili, A. D., and Yu, F. M., "Investigation of the Interacting Flow of Nonsymmetric Jets in Crossflow," *AIAA Journal*, Vol. 26, No. 8, 1988, pp. 940–947.

[3]Johnston, J. P., and Nishi, M., "Vortex Generator Jets—Means for Flow Separation Control," *AIAA Journal*, Vol. 28, No. 6, 1990, pp. 989–994.

[4]Lin, J. C., Howard, F. G., and Selby, G. V., "Investigation of Several Passive and Active Methods for Turbulent Flow Separation Control," AIAA Paper 90-1598, June 1990.

[5]Compton, D. A., and Johnston, J. P., "Streamwise Vortex Production by Pitched and Skewed Jets in a Turbulent Boundary Layer," *AIAA Journal*, Vol. 30, No. 3, 1992, pp. 640–647.

[6]Selby, G. V., Lin, J. C., and Howard, F. G., "Control of Low-Speed Turbulent Separated Flow Using Jet Vortex Generators," *Experiments in Fluids*, Vol. 12, 1992, pp. 394–400.

[7]Honami, S., Shizawa, T., and Uchiyama, A., "Behavior of the Laterally Injected Jet in Film Cooling: Measurements of Surface Temperature and Velocity/Temperature Field Within the Jet," *Journal of Turbomachinery*, Vol. 116, Jan. 1994, pp. 106–112.

[8]Zhang, X., "Turbulence Measurements of a Longitudinal Vortex Generated by an Inclined Jet in a Turbulent Boundary Layer," *Journal of Fluids Engineering*, Vol. 120, Dec. 1998, pp. 765–771.

[9]Johnston, J. P., and Khan, Z., "The Origins of the Dominant Vortex From a Pitched and Skewed Jet," *Proceedings of the International Conference on Fluids Engineering*, Vol. 1, No. 97-203, Tokyo, 1997, pp. 321–326.

[10]Khan, Z. U., and Johnston, J. P., "On Vortex Generating Jets," *International Journal of Heat and Fluid Flow*, Vol. 21, 2000, pp. 506–511.

[11]Johnston, J. P., Mosier, B. P., and Khan, Z. U., "Effects of Inlet Conditions on Skewed and Pitched Jets in Cross-Flow," *2nd International Symposium on Turbulent Shear Flow Phenomena*, Stockholm, 2001, pp. 1–6.

[12]Johnston, J. P., "Pitched and Skewed Vortex Generator Jets for Control of Turbulent Boundary Layer Separation: A Review," *Proceedings of the 3rd ASME/JSME Joint Fluids Engineering Conference*, San Francisco, 1999, pp. 1–10.

[13]Bray, T. P., "A Parametric Study of Vane and Air-Jet Vortex Generators," Ph.D. Dissertation, Flow Control and Prediction Group, College of Aeronautics, Cranfield Univ., Cranfield, England, U.K., Oct. 1998.

[14]Bray, T. P., and Garry, K. P., "Optimization of Air-Jet Vortex Generators with Respect to System Design Parameters," *Aeronautical Journal*, Oct. 1999, pp. 475–479.

[15]Milanovic, I. M., and Zaman, K. B. M. Q., "Highly Inclined Jets in Cross-Flow," AIAA Paper 2003-0183, Jan. 2003.

[16]Foss, J. K., and Zaman, K. B. M. Q., "Large- and Small-Scale Vortical Motion in a Shear Layer Perturbed by Tabs," *Journal of Fluid Mechanics*, Vol. 382, 1999, pp. 307–329.

[17]Lee, S. W., Lee, J. S., and Ro, S. T., "Experimental Study on the Flow Characteristics of the Streamwise Inclined Jets in Crossflow on Flat Plate," *International Gas Turbine and Aeroengine Congress and Exposition*, Cologne, Germany, 1992, pp. 1–9.

[18]Gopalan, S., Abraham, B., and Katz, J., "Turbulent Jet Injected into a Cross Flow—Analysis of the Flow Structure and Wall Pressure Fluctuations," American Society of Mechanical Engineers, Paper FEDSM2002-31420, July 2002.

[19]Bandypadyay, P. R., Stead, D. J., and Ash, R. L., "Organized Nature of a Turbulent Trailing Vortex," *AIAA Journal*, Vol. 29, No. 10, 1991, pp. 1627–1633.

[20]Leibovich, S., "Vortex Stability and Breakdown: Survey and Extension," *AIAA Journal*, Vol. 22, No. 9, 1984, pp. 1192–1206.

[21]Wang, F. Y., Milanovic, I. M., and Zaman, K. B. M. Q., "A Quantitative Comparison of Leading-Edge Vortices in Incompressible and Supersonic Flows," AIAA Paper 2002-0557, Jan. 2002.

W. Devenport
Associate Editor